PAPER

Experimental creation and analysis of displaced number states

To cite this article: F Ziesel *et al* 2013 *J. Phys. B: At. Mol. Opt. Phys.* **46** 104008

J. Phys. B: At. Mol. Opt. Phys. **46** (2013) 104008 (6pp) doi:10.1088/0953-4075/46/10/104008

Experimental creation and analysis of displaced number states

F Ziesel, T Ruster, A Walther, H Kaufmann, S Dawkins, K Singer, F Schmidt-Kaler and U G Poschinger

QUANTUM, Institut für Physik, Universität Mainz, Staudingerweg 7, D-55128 Mainz, Germany

E-mail: poschin@uni-mainz.de

Received 19 November 2012, in final form 13 January 2013
Published 9 May 2013
Online at stacks.iop.org/JPhysB/46/104008

Abstract

We create displaced number states, which are non-classical generalizations of coherent states, of a vibrational mode of a single trapped ion. The creation of these states is accomplished by a combination of optical and electrical manipulation of the ion. A number state is first prepared by laser-driven climbing of the Jaynes–Cummings ladder, followed by displacement created by a sudden shift of the electrostatic trapping potential. Number states $n = 0$, 1 and 2 are prepared, and displacement amplitudes of up to $\alpha \approx 2.8$ are reached. The states are analysed by the experimental reconstruction of the number state distribution, and we find good agreement with the theoretically expected results for displaced number states. Quantum features elucidating the concept of interference in phase space are clearly demonstrated experimentally.

(Some figures may appear in colour only in the online journal)

1. Introduction

Over the last few years, it has become possible to perform experiments on well-isolated simple quantum systems. For example, a trapped single ion can be manipulated with laser interactions such that non-classical states of the ion's internal electronic and external vibrational states can be created and probed. Such experiments allow for exploring the fascinating features of quantum entanglement [1, 2] and have set the basis for emerging quantum technologies, e.g. scalable quantum processors using ions in a segmented ion trap device [3]. Engineering and probing non-classical states of quantum systems, besides being of interest in its own right, has many prospects and applications. Techniques for quantum control and measurement can be established and benchmarked, decoherence properties of different quantum states can be compared [4] and theoretical concepts such as the negativity of quasi-probability distributions can be studied. Furthermore, nonclassical states set the ground for quantum simulation experiments [5, 6] and offer the possibility of enhanced interferometric resolution [7], providing the basis for future quantum sensors.

An example of a nonclassical state is the displaced number state (DNS), which is a generalization of the well-known Glauber coherent state. The DNS can be represented as $|\alpha, n\rangle$ in Dirac notation, where n is the quantum number of an energy eigenstate of a harmonic oscillator, which is additionally displaced by an amplitude α in phase space. DNSs have been studied theoretically [8–11], and they provide a versatile tool e.g. for the calculation of quasi-probability distributions, as their coherent or number state nature can be exploited depending on the context. Furthermore, the DNS provides a clear illustration of the concept of *interference in phase space* [12], e.g. yielding a semiclassical explanation of molecular spectra. Experimental work on the DNS performed so far with photons includes generation and characterization of the state $|\alpha, 1\rangle$ with displacements of up to $\alpha \approx 2.4$ [13], which revealed clear deviations from the ordinary coherent state $|\alpha, 0\rangle$, and signatures of interference in phase space have been observed. A more recent experiment with photons showed the non-classical decrease of the overlap integral $|\langle 1|\alpha, 1\rangle|^2$ with increasing α [14]. Further experimental work established an analogy between the DNS and classical light propagation in Glauber–Fock waveguides [15, 16].

For trapped ions, many fascinating experiments have been performed on the generation and analysis of nonclassical states over the last two decades, prominent examples being the creation of Fock, coherent and squeezed states [17], the tomographic reconstruction of quasi-probability distributions [18] and more recently the entanglement of the motional

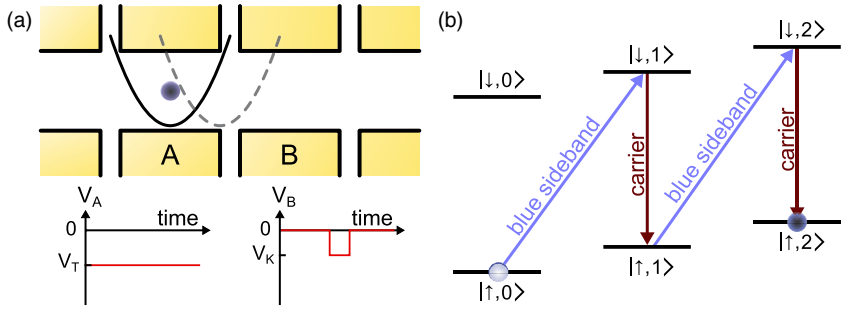

Figure 1. State preparation scheme: (a) shows how controlled displacement is achieved by switching the voltage of the trap segments. The ion is initially kept at segment A, while a voltage pulse on segment B temporarily shifts the potential minimum. The voltage ramp is performed such that the ion cannot adiabatically follow the displaced potential minimum. (b) illustrates the preparation of number states by alternating π-pulses on blue sideband and carrier transitions.

modes of two trapped ions [19]. Displacement of vibrational states has also been performed with neutral atoms in an optical lattice [20]. Our work extends the previous work on nonclassical states of trapped ions by adding the DNS to the collection of states generated and analysed so far. While photonic experiments have been limited to states $|\alpha, 1\rangle$, we prepare states of up to $n = 2$ and are able to see characteristic higher order interference minima in phase space. In addition, we demonstrate that both optical and non-resonant electrical forces can be applied together with sufficient precision to allow for quantum state engineering of the motional degree of freedom. We did not perform a direct phonon number measurement, compared to the direct photon number detection in [14]. Instead, we partially reconstruct the generated state of the motional mode of a single trapped ion by the determination of the number state distribution. We achieve a precise matching of the obtained results to the theoretical prediction.

2. Experimental scheme

2.1. Preparation of displaced Fock states

To create the DNS of the axial mode of vibration of a single trapped ion, we combine different methods for the quantum control of motional and internal degrees of freedom. We first create number states by a sequence of laser pulses consisting of π pulses on the blue motional sideband, each adding a phonon to the motional excitation, and π pulses on the carrier transition to reset the internal state. Electrical forces generated with control voltages at the trap segments are then used to displace the harmonic oscillator by a well-defined amplitude. The scheme is sketched in figure 1. The displacement operation is realized by the rapid change of the trapping voltages applied to the trap segments. This is done by means of a custom-built fast arbitrary waveform generator. Such hardware technology with sufficient precision and low noise level became available only recently, enabling the fast transport of a trapped ion over long distances [21, 22]. We note that the displacement can also be accomplished by different means. One possibility is the application of optical forces [1]; here the magnitude of achievable displacement is limited by the requirement that the oscillation amplitude in position space has to be well below the wavelength of the optical driving field [23]. Another possibility is resonant electrical driving [18].

The detailed experimental scheme is as follows: a single $^{40}Ca^{+}$ ion is stored in a microstructured segmented Paul trap [24] and laser cooled on the $S_{1/2} \leftrightarrow P_{1/2}$ cycling transition near 397 nm. The $m_J = -1/2$ and $m_J = +1/2$ sublevels of the $S_{1/2}$ ground state are henceforth termed $|\uparrow\rangle$ and $|\downarrow\rangle$, respectively. These levels are split in energy by an external magnetic field, leading to a Zeeman splitting of about $\omega_Z \approx 2\pi \cdot 18$ MHz. Coherent transitions between these states are driven via stimulated Raman transitions [25]. These transitions are mediated via the $P_{1/2}$ state and driven by two optical fields near 397 nm, red detuned from the cycling transition by a frequency of about $\Delta_R \approx 2\pi \cdot 40$ GHz. Coupling to the axial mode of vibration takes place with a Lamb–Dicke factor of about $\eta \approx 0.21$ [26], allowing for the coherent driving of motional sidebands.

For each measurement, the axial mode of vibration at a frequency of $\omega_{ax} \approx 2\pi \cdot 1.35$ MHz is cooled close to the motional ground state with pulsed Raman sideband cooling on a stimulated Raman transition, reaching a mean phonon number as low as $\bar{n} \leqslant 0.1$. The internal state is then initialized to $|\uparrow\rangle$ by optical pumping. We then prepare a Fock state $|n\rangle$ by performing a π-pulse on the blue motional sideband of the stimulated Raman transition, changing the state according to

$$|\uparrow, m\rangle \rightarrow |\downarrow, m+1\rangle. \quad (1)$$

The internal state is then reset by a π-pulse on the carrier transition,

$$|\downarrow, m+1\rangle \rightarrow |\uparrow, m+1\rangle. \quad (2)$$

This sequence is repeated n times. For each Fock state preparation step m, the pulse areas for the sideband and carrier pulses are calibrated by monitoring the respective Rabi oscillations. The preparation is concluded by additional optical pumping to $|\uparrow\rangle$ with a circularly polarized beam at the cycling transition. The fidelity of the Fock state preparation is limited by the imperfect preparation of the motional ground state, leading to a fidelity deterioration for higher n, since the transfer pulse areas depend on m and are therefore not well defined. This results in a spread of the population over the state ladder. This error can be partially compensated by a concluding optical pumping, which facilitates the evaluation of the data by setting a well-defined internal state of the ion. However, deviations of the desired final motional quantum number are not compensated; this error is even slightly increased as there

is a finite probability of changing the motional state in an excitation and decay cycle of the pumping.

The displacement is then performed by changing the voltage levels on the trap segment and its neighbouring segment; further details are explained in section 2.3. The voltages are switched back to the initial values after 400 ns. We then apply an analysis laser pulse of variable duration on the stimulated Raman transition and its respective blue and red sidebands. The analysis procedure is further detailed in section 2.2. Finally, the population in $|\uparrow\rangle$ is selectively transferred to the metastable $D_{5/2}$ state by electron shelving with laser light near 729 nm. Upon subsequent saturated driving of the cycling transition, fluorescence will be observed if the ion is found to be in the $|\downarrow\rangle$ state before the shelving, and no fluorescence will be observed otherwise, such that a spin-selective readout is performed. The entire sequence is repeated 200 times to obtain an estimate of the probability $P_\uparrow$ to be in the $|\uparrow\rangle$ state. This measurement is carried out for various analysis pulse durations and analysis pulse detunings, corresponding to resonant driving of the red sideband, carrier and blue sideband.

2.2. State analysis

We describe the motional state of the ion, which is not necessarily a pure state, by the density matrix $\hat{\rho}$. We assume the preparation of the internal state $|\uparrow\rangle$; thus the total state is given by $|\uparrow\rangle \otimes \hat{\rho}$ prior to the analysis pulse. The analysis pulse resonantly drives transitions, altering the motional state by Δn phonons in one excitation step, where $\Delta n = +(-)1$ denotes the blue(red) sideband and $\Delta n = 0$ corresponds to the carrier. The final probability of finding the ion in the $|\uparrow\rangle$ state is then given by the Rabi oscillation signal

$$P_{\uparrow,\Delta n}(\theta) = \frac{1}{2}\sum_{k=0}^{k_{\max}} p_k(1+\cos(M_{k,\Delta n}\theta)), \tag{3}$$

where θ indicates the analysis pulse area and $p_k = \mathrm{Tr}(\hat{\rho}|k\rangle\langle k|)$ is the phonon probability distribution (PPD). This is a sum of Rabi oscillations starting from different number states k, where the Rabi frequency is altered by the matrix element $M_{k,\Delta n}$ [26] in a nonlinear way. This opens up the possibility of infering p_k from the measured signal. The reconstruction of the PPD from a set of measured functions, $P_\uparrow(\theta)$, with $\Delta n = -1, 0, 1$, is done with a maximum likelihood parameter estimation, where the p_k values for $k \leqslant k_{\max} = 6$ are varied freely, besides the requirement of a normalized PPD. Further parameters such as the bare Rabi frequency and the readout fidelity are included in the reconstruction to suppress systematic errors.

2.3. Controlled displacement by fast voltage switching

The displacement operation $|n\rangle \rightarrow \hat{D}(\alpha)|n\rangle = |\alpha, n\rangle$ is performed by switching the voltage on the neighbouring segment to the trap segment, with its centre located 280 μm away from the initial trap position. A voltage of 1.0 V at this segment will give rise to an electric field of about 600 V m^{-1} at the initial ion location, which is derived from electrostatic simulation of the trap [27]. This field exerts an acceleration of approximately 1.5×10^9 m s^{-2}. Assuming an ideal, sudden switching process, the potential minimum is shifted by a well-defined distance along the trap axis for a well-defined time. The relation between the set voltage and the magnitude of the shift of the potential minimum is established via electrostatic simulation of the trap and has been experimentally confirmed [28]. For the displacement, the set voltage is changed instantaneously; however, Π-type filters with cutoff frequencies of approximately 300 kHz lead to smoothened voltage ramps at the trap segment. The actual displacement amplitude after the voltage kick is therefore lower than the value corresponding to the position space shift of the potential minimum; furthermore, the displacement pulse is delayed and blurred. With the deviation of the minimum potential from its original location $x_0(t)$, the resulting displacement is obtained from classical harmonic oscillator dynamics [21]:

$$\alpha(t) = -\sqrt{\frac{m\omega}{2\hbar}}\left(\mathrm{e}^{-\mathrm{i}\omega t}\int_0^t \dot{x}_0(\tau)\mathrm{e}^{\mathrm{i}\omega\tau}\mathrm{d}\tau\right). \tag{4}$$

The fast switching of the voltages is done with a fast multichannel arbitrary waveform generator. Its main building blocks are quad 16-bit serial digital to analogue converters[1], which cover the output voltage range of −10 to +10 V with a resolution of about 0.3 mV. The digital data are supplied in real time by a field programmable gate array (FPGA)[2], which in turn is programmed via a Gigabit Ethernet connection from a control computer. The maximum update rate is limited by the clock rate of the FPGA and is given by 2.5 MSamples s^{-1}, and a number of up to 48 output channels can be controlled individually. A crucial feature is the possibility of varying the duration of each individual sample in steps of 10 ns beyond the minimum value of 400 ns, which allows for resolving the trap oscillation period [22].

Each output channel at voltage V_i is fed into a stage where a differential voltage V_d is added (subtracted) such that two channels with output voltages $V_i \pm V_d$ are obtained, which are fed to segments at the same axial location in the trap, which allow for the compensation of micromotion. The differential voltage V_d can be derived from a DAC or from an external input.

The measured output voltage noise at the trap frequency, in the steady state, is as low as 1.0×10^{-9} V Hz$^{-1/2}$. This results in a spectral density of the electric field noise of about 3.6×10^{-13} V^2 Hz^{-1} m^{-2}, which in turn yields a heating rate lower than the actually observed heating rate of $\dot{n} \approx 0.3$ ms^{-1}[25] by one order of magnitude; it therefore does not significantly contribute to the anomalous heating. Care was taken to suppress digital noise, i.e. feedthrough of the FPGA clock and other digital signals onto the output channels is reduced by using high-speed magnetic insulators for all digital signal lines and careful separation of analogue and digital signals on the circuit boards bearing the DACs.

We predict the resulting displacement magnitudes from simulations, which take into account the actual voltage waveforms applied to the shift segment. These waveforms are measured behind the filter. Averaging of about 1000 identically

[1] DAC8814, Texas Instruments.
[2] Avnet Virtex-5 FXT Evaluation Kit.

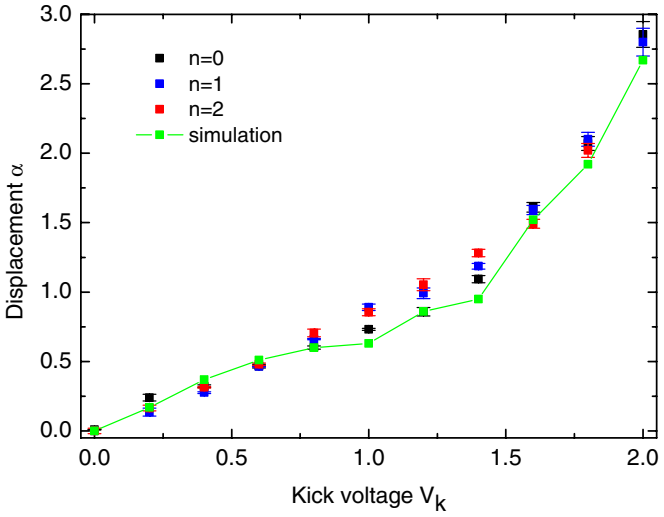

Figure 2. Extracted values for the displacement parameter α versus the kick voltage V_k for the datasets pertaining to $n = 0$ (black), $n = 1$ (blue) and $n = 2$ (red). The displacement parameters are obtained by fitting the theoretical prediction (equation (7)) to the reconstructed PPDs. The curves are clearly consistent, providing justification for the evaluation method. A slight deviation is observed for the $n = 0$ case, which we attribute to a slow drift of the trap voltages. The green points show results from simulations, which are connected by solid lines to guide the eye.

generated waveforms was necessary to make the results independent of measurement artefacts. These waveforms are used in conjunction with the simulated electrostatic potentials for the numerical solution of the classical equation of motion,

$$m\ddot{x} = -eU_A \frac{\mathrm{d}V_A^{(1V)}}{\mathrm{d}x} - eU_B(t) \frac{\mathrm{d}V_B^{(1V)}}{\mathrm{d}x}, \tag{5}$$

where the forces are given by the spatial derivatives of the normalized electrostatic potentials $V_i^{(1V)}(x)$ along the trap axis, which result from a segment voltage of 1 V applied to electrode i. These forces are weighted by the respective voltages applied to the electrodes and added. The final energy E_f at times larger than the settling time is rescaled to harmonic oscillator units, $E'_f = E_f/\hbar\omega$, and the displacement is obtained from $|\alpha| = \sqrt{E'_f}$. The resulting displacement amplitudes versus the kick amplitude V_k are shown in figure 2. Larger displacement values can in principle be easily achieved by further increasing the kick voltage. Even for a limited voltage range, resonantly exciting the motional mode would allow for attaining macroscopic oscillation amplitudes. However, the limit in extracting DNS characteristics from the Rabi oscillation data is imposed by the reconstruction procedure explained in section 2.2. Extending the Hilbert space used for the reconstruction of the PPD to larger truncation values $k_{\max}$ deteriorates the fidelity of the reconstruction; this effect is enhanced by the fact that the relative variation of Rabi frequencies becomes smaller for increasing vibrational quantum numbers.

3. Results

With the optically driven ladder climbing method described above, we prepare number states for $n = 0, 1, 2$ before applying the kick. The displacement is determined by the magnitude of the voltage kick on the neighbouring segment. The kick voltage V_k is changed in steps of 200 mV, reaching a maximum displacement of $\alpha \approx 2.8$ at $V_k = 2$ V. In each case, the state reconstruction is performed with freely varying PPD. As a result, we obtain a normalized PPD for each pair of n and α. The results for $n = 1$ are shown in figure 3. The measured PPD is compared to the theoretically expected one [8, 9],

$$p_k^{(n)} = |\langle k|\alpha, n\rangle|^2 = \mathrm{e}^{-|\alpha|^2} |\alpha|^{2(k-n)} n!k! \times \left| \sum_{l=0}^{n} \frac{(-1)^l |\alpha|^{2(n-l)}}{l!(n-l)!(k-l)!} \right|^2 . \tag{6}$$

We take into account the imperfect preparation of the desired number state prior to the displacement operation.

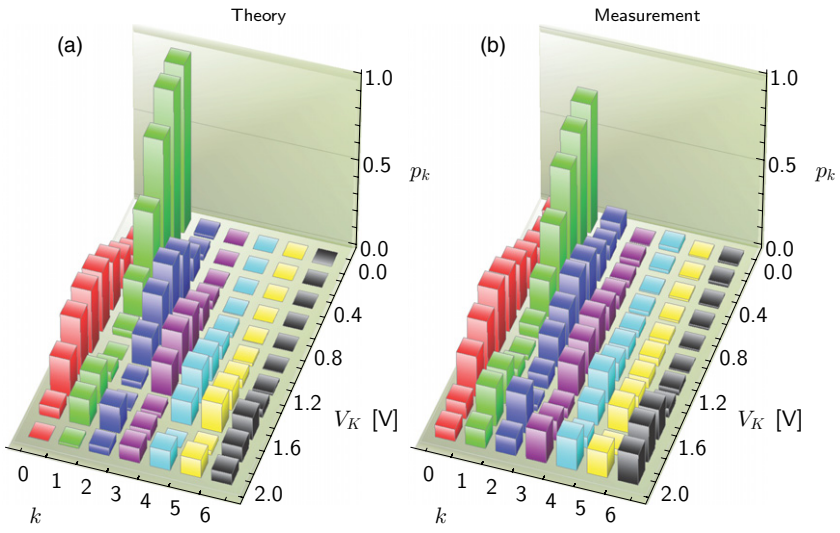

Figure 3. Resulting theoretical PPD (a) and PPD reconstructed from the measurement result (b) for the preparation of $n = 1$. The PPDs are shown for each applied kick voltage. The interference minimum is clearly observable as a ditch bending towards higher phonon numbers for larger kick voltages.

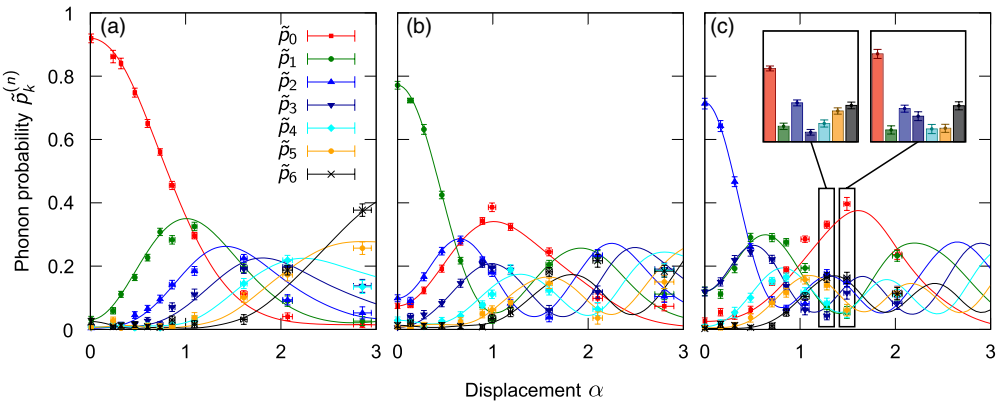

Figure 4. Resulting PPDs for different number state preparations (a) $n = 0$, (b) $n = 1$ and (c) $n = 2$. The respective PPDs are plotted versus the displacement amplitude α, which in turn is extracted by fitting the PPD to equation (6). The solid lines display the theoretically expected values from the same equation (6). The matching of the experimental values to the theoretical values becomes worse for larger displacement amplitudes because the precision of the maximum likelihood reconstruction is deteriorated by truncation errors. The insets for the $n = 2$ case show the PPDs at $\alpha \approx 1.3$ and $\alpha \approx 1.5$, which show the interference minima.

We assume that the action of the displacement kick is not dependent on the quantum state of the motional mode, which is justified by the spatial homogeneity of the electrical force. We characterize the motional mode after the preparation of the desired Fock state n, i.e. the state corresponding to zero kick voltage, by the PPD $q_m^{(n)}$. For each prepared n, $q_m^{(n)}$ is obtained from measurement data. We obtain the PPD which is actually measured from a convolution of the pure PPD from equation (6) with $q_m^{(n)}$:

$$\tilde{p}_k^{(n)} = \sum_{m=0}^{n_{\max}} q_m^{(n)} p_k^{(m)}. \tag{7}$$

From the reconstructed PPDs $q_m^{(n)}$ without a kick, we determine the respective Fock state preparation fidelities $q_0^{(0)} \approx 0.92$, $q_1^{(1)} \approx 0.77$ and $q_2^{(2)} \approx 0.72$.

For nonzero kick voltages, the corresponding displacement parameter α is extracted from the PPD equation (7), where the theoretical PPD equation (6) is employed. By least-squares minimization, we obtain the value for α which provides the best matching to the experimental values. To prove the consistency of this evaluation method, we show the extracted displacement magnitudes α versus the kick voltage V_k for the three different datasets in figure 2. When these values are compared to displacement values inferred from simulations, we find agreement on the single quantum level.

In figure 3, we show the resulting PPDs for the case $n = 1$ plotted versus the kick voltage. The results clearly exhibit a single minimum in the PPD, which is shifted to higher phonon numbers for larger kick voltages. The occurrence of two minima in the PPD is visible for $n = 2$ (see figure 4, insets), which has not been observed before in photonic realizations of the DNS. The fact that n minima can occur in the PPD of a state $|\alpha, n\rangle$ can be directly read off from equation (6): within the sum a polynomial of order n in $|\alpha|^2$ with coefficients of alternating signs is formed, which maximally exhibits n zeros upon squaring [9].

To provide a semiclassical explanation for the occurrence of the minima, we illustrate the idea of interference in phase space in figure 5 [29]. In phase space, number states $|n\rangle$ are represented by circular bands of nonzero probability density, where the radius increases with n. Displacement is represented by a shift of the centre of these bands away from the origin. The overlap integral $\langle k|\alpha, n\rangle$ is given by the coherent sum of the two intersection areas A between the bands representing the number states $|k\rangle$ and $|n\rangle$. In the summation, one has to take into account the relative phase $\phi_{nk}(\alpha) = B/\hbar$ which is given by the area B enclosed between the two classical trajectories:

$$|\langle k|\alpha, n\rangle|^2 = \frac{2}{\pi\hbar} \cos\phi_{nk}(\alpha). \tag{8}$$

As the preparation number n increases, the values of $\phi_{nk}(\alpha)$ sweep over larger ranges for increasing analysis quantum

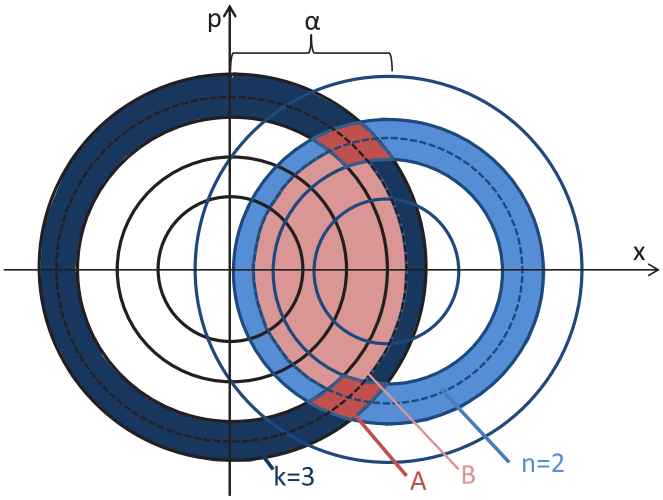

Figure 5. Illustration how interference in phase space leads to the observed minima in the PPDs. We exemplify the overlap integral $\langle 3|\alpha, 2\rangle$. The Fock states are represented semiclassically as bands in phase space, spread around the classical trajectories corresponding to the energy eigenvalues $(n + 1/2)\hbar\omega$ (dashed lines). The analysis number state basis is represented by bands centred around the origin, and the DNS states $|\alpha, n\rangle$ are displaced by the amplitude α. The overlap integral is determined not only by the diamond shaped red areas A, but also by the intersection area B of the trajectories (shaded in light red), see the text.

numbers k and increasing α, thus allowing for a larger number of interference minima.

4. Outlook and conclusion

We have demonstrated the creation of a DNS $|\alpha, n\rangle$ with number states of up to $n = 2$ and $\alpha \approx 2.8$, going significantly beyond the current state of the art of photonic experiments performed on the DNS so far. Emphasis is given on the fact that the displacement is created by electrical kicks, not by resonant excitation by rf-pulses. This offers the flexibility to combine long-distance shuttling operations and controlled motional excitation on the single quantum accuracy level, which might open up the route to scalable quantum simulation schemes. The displacement operations were shown to be very accurate and reproducible. We emphasize that we were able to match the measured displacement amplitudes to simulation results with an accuracy better than the single quantum level, where technological details such as the electrostatic properties of the microtrap and the voltage waveforms have to be determined with a sufficient precision.

Future applications in the field of quantum state engineering include the joint usage of spin-dependent optical forces and electrical forces, e.g. for optically assisted splitting of ion crystals or for phase referencing optical beat patterns. The latter might open up the possibility for novel measurement schemes where an optical interference pattern may be applied with a fixed phase relation to ion strings [30], which could be of use for quantum simulation experiments [31].

Acknowledgments

The authors acknowledge gratitude to Heinz Lenk for the development of electronics hardware. We acknowledge financial support by the IARPA SQIP project (MQCO framework), and by the European commission within the IP AQUTE, STREP Diamant and the VW-Stiftung. AW acknowledges funding from the Swedish Research Council.

References

[1] Monroe C, Meekhof D M, King B E and Wineland D J 1996 *Science* **272** 1131
[2] Deléglise S, Dotsenko I, Sayrin C, Bernu J, Brune M, Raimond J M and Haroche S 2008 *Nature* **455** 510
[3] Kielpinski D, Monroe C and Wineland D 2002 *Nature* **417** 709
[4] Barreiro J T, Schindler P, Gühne O, Monz T, Chwalla M, Roos C F, Hennrich M and Blatt R 2010 *Nature Phys.* **6** 943
[5] Leibfried D *et al* 2002 *Phys. Rev. Lett.* **89** 247901
[6] Gerritsma R, Kirchmair G, Zähringer F, Solano E, Blatt R and Roos C F 2010 *Nature* **463** 68
[7] Caves C M 1981 *Phys. Rev.* D **23** 1693
[8] Boiteux M and Levelut A 1973 *J. Phys. A: Math. Nucl. Gen.* **6** 589
[9] de Oliveira F A M, Kim M S, Knight P L and Buzek V 1990 *Phys. Rev.* A **41** 2645
[10] Wünsche A 1991 *Quantum Opt.* **3** 359
[11] Moya-Cessa H 1995 *J. Mod. Opt.* **42** 1741
[12] Dowling J P, Schleich W P and Wheeler J A 1991 *Ann. Phys.* **48** 423
[13] Lvovsky A I and Babichev S A 2002 *Phys. Rev.* A **66** 011801
[14] Laiho K, Cassemiro K N, Gross D and Silberhorn C 2010 *Phys. Rev. Lett.* **105** 253603
[15] Perez-Leija A, Moya-Cessa H, Szameit A and Christodoulides D N 2010 *Opt. Lett.* **35** 2409
[16] Keil R, Perez-Leija A, Dreisow F, Heinrich M, Moya-Cessa H, Nolte S, Christodoulides D N and Szameit A 2011 *Phys. Rev. Lett.* **107** 103601
[17] Meekhof D M, Monroe C, King B E, Itano W M and Wineland D J 1996 *Phys. Rev. Lett.* **76** 1796
[18] Leibfried D, Meekhof D M, King B E, Monroe C, Itano W M and Wineland D J 1996 *Phys. Rev. Lett.* **77** 4281
[19] Jost J D, Home J P, Amini J M, Hanneke D, Ozeri R, Langer C, Bollinger J J, Leibfried D and Wineland D J 2009 *Nature* **459** 683
[20] Maneshi S, Kanem J F, Zhuang C, Partlow M and Steinberg A M 2008 *Phys. Rev.* A **77** 022303
[21] Bowler R, Gaebler J, Lin Y, Tan T R, Hanneke D, Jost J D, Home J P, Leibfried D and Wineland D J 2012 *Phys. Rev. Lett.* **109** 080502
[22] Walther A, Ziesel F, Ruster T, Dawkins S T, Ott K, Hettrich M, Singer K, Schmidt-Kaler F and Poschinger U G 2012 *Phys. Rev. Lett.* **109** 080501
[23] Poschinger U G, Walther A, Singer K and Schmidt-Kaler F 2010 *Phys. Rev. Lett.* **105** 263602
[24] Schulz S, Poschinger U, Ziesel F and Schmidt-Kaler F 2008 *New J. Phys.* **10** 045007
[25] Poschinger U G *et al* 2009 *J. Phys. B: At. Mol. Opt. Phys.* **42** 154013
[26] Leibfried D, Blatt R, Monroe C and Wineland D 2003 *Rev. Mod. Phys.* **75** 281–324
[27] Singer K, Poschinger U, Murphy M, Ivanov P, Ziesel F, Calarco T and Schmidt-Kaler F 2010 *Rev. Mod. Phys.* **82** 2609–32
[28] Huber G, Ziesel F, Poschinger U G, Singer K and Schmidt-Kaler F 2010 *Appl. Phys.* B **100** 725
[29] Schleich W 2001 *Quantum Optics in Phase Space* (Berlin: Wiley-VCH)
[30] Walther A, Poschinger U G, Singer K and Schmidt-Kaler F 2012 *Appl. Phys.* B **107** 1061
[31] Pruttivarasin T, Ramm M, Talukdar I, Kreuter A and Häffner H 2011 *New J. Phys.* **13** 075012